1854 *Chem. Mater.* **2010,** *22,* 1854–1861
DOI:10.1021/cm903370z

CHEMISTRY OF MATERIALS
Article

Structural and Electrochemical Study of a New Crystalline Hydrated Iron(III) Phosphate $FePO_4 \cdot H_2O$ Obtained from $LiFePO_4(OH)$ by Ion Exchange

Nicolas Marx,[†] Laurence Croguennec,*[,†] Dany Carlier,[†] Lydie Bourgeois,[‡] Pierre Kubiak,[†] Frédéric Le Cras,[§] and Claude Delmas[†]

[†]*ICMCB-CNRS, Université de Bordeaux, IPB-ENSCBP - 87 av. Schweitzer, 33608 Pessac cedex, France,* [‡]*Université de Bordeaux, ISM - 351 cours de la Libération, 33405 Talence cedex, France, and* [§]*CEA, LITEN - 17 av. des Martyrs, 38054 Grenoble cedex, France*

Received November 4, 2009. Revised Manuscript Received December 16, 2009

A new iron(III) phosphate $FePO_4 \cdot H_2O$, isostructural to already reported $VPO_4 \cdot H_2O$ and $MnPO_4 \cdot H_2O$ phases, was obtained from tavorite $LiFePO_4(OH)$ through a Li^+/H^+ exchange. The composition of this new phase was confirmed by different chemical analyses. The ion-exchange reaction was shown to be topotactic; indeed the structures of $LiFePO_4OH$ and $FePO_4 \cdot H_2O$ are very similar and both are characterized by chains of FeO_6 octahedra, interconnected through PO_4 tetrahedra, such as the resulting frameworks enclose different types of tunnels. A neutron diffraction study has allowed the localization of hydrogens in the $FePO_4 \cdot H_2O$ structure, revealing that the two hydrogen atoms are linked to the oxygen atoms shared by two adjacent FeO_6 octahedra. The presence of these "H_2O-like" groups inserted along the FeO_6 chains leads to a considerable distortion of the FeO_6 octahedra. The nature of the $-OH$ and $-OH_2$ groups in $LiFePO_4OH$ and $FePO_4 \cdot H_2O$, respectively, was confirmed by vibrational spectroscopies. Lithium intercalation was shown to occur in $FePO_4 \cdot H_2O$ through the reduction of Fe^{3+} to Fe^{2+} at an average voltage of ~2.8 V (vs Li^+/Li) with a good cyclability.

Introduction

During the past decade, polyanionic three-dimensional structures built of XO_4 tetrahedra and MO_6 octahedra have been intensively studied for their potential application as electrode material for lithium-ion batteries. The olivine $LiFePO_4$ compound, which is now used in commercial lithium-ion batteries, has crystallized most of the research efforts due to its attractive properties.[1−8]

The high interest for phosphate materials and especially for $LiFePO_4$ is linked to their structural stability both in the intercalated and deintercalated form, which is due to the presence of iron in two very stable oxidation states (i.e., Fe^{2+} and Fe^{3+}). Indeed, on the contrary to the lithium transition metal oxides $LiMO_2$[9] no oxygen loss occurs at high temperature for highly deintercalated Li_xFePO_4; only phase degradation is observed.[10] This iron-based phosphate material is thus very attractive not only from a safety point of view (limited gas generation) but also for its low cost and good performance upon long-range cycling. More recently, the interest moved to Fe, Mn, and V-based fluorophosphate materials with the aim to overcome the limitation of the low potential of $LiFePO_4$ (3.45 V vs Li^+/Li) and reach a higher energy density.[11−15] Indeed, the higher electronegativity of fluorine allows increasing the ionicity of the M−O(F) bonds and thus the redox potential of the transition metal couple. In this context we were recently interested in the tavorite system $LiFePO_4(OH)$ and especially in the possibility to form the isostructural $LiFePO_4F$ phase,[16] as observed for the aluminum system $LiAlPO_4(OH,F)$.[17]

*Corresponding author phone: +33 (0) 5 4000 2234 (or 2647); fax: +33 (0) 5 4000 2761; e-mail: crog@icmcb-bordeaux.cnrs.fr.

(1) Padhi, A. K.; Nanjundaswamy, K. S.; Goodenough, J. B. *J. Electrochem. Soc.* **1997**, *144*, 1188.
(2) Ravet, N.; Chouinard, Y.; Magnan, J. F.; Besner, S.; Gauthier, M.; Armand, M. *J. Power Sources* **2001**, *97*−*8*(Special Iss. SI), 503.
(3) Huang, H.; Yin, S. C.; Nazar, L. F. *Electrochem. Solid-State Lett.* **2001**, *4*, A170.
(4) Yamada, A.; Yonemura, M.; Takei, Y.; Sonoyama, N.; Kanno, R. *Electrochem. Solid-State Lett.* **2005**, *8*(1), A55.
(5) Chen, G. Y.; Song, X. Y.; Richardson, T. J. *Electrochem. Solid-State Lett.* **2006**, *9*(6), A295.
(6) Laffont, L.; Delacourt, C.; Gibot, P.; Wu, M. Y.; Kooyman, P.; Masquelier, C.; Tarascon, J. M. *Chem. Mater.* **2006**, *18*, 5520.
(7) Delmas, C.; Maccario, M.; Croguennec, L.; Le Cras, F.; Weill, F. *Nat. Mater.* **2008**, *7*, 665.
(8) Ramana, C. V.; Mauger, A.; Gendron, F.; Julien, C. M.; Zaghib, K. *J. Power Sources* **2009**, *187*, 555.
(9) Guilmard, M.; Croguennec, L.; Delmas, C. *Chem. Mater.* **2003**, *15*, 4484.
(10) Delacourt, C.; Poizot, P.; Tarascon, J.-M.; Masquelier, C. *Nat. Mater.* **2005**, *4*, 254.
(11) Barker, J.; Saidi, M. Y.; Swoyer, J. L. *J. Electrochem. Soc.* **2003**, *150*, A1394.
(12) Barker, J.; Saidi, M. Y.; Swoyer, J. L. *J. Electrochem. Soc.* **2004**, *151*, A1670.
(13) Barker, J.; Gover, R. K. B.; Burns, P.; Bryan, A.; Saidi, M. Y.; Swoyer, J. L. *J. Electrochem. Soc.* **2005**, *152*(A), 1776.
(14) Makimura, Y.; Cahill, L. S.; Iriyama, Y.; Goward, G. R.; Nazar, L. F. *Chem. Mater.* **2008**, *20*(13), 4240.
(15) Ellis, B. L.; Makahnouk, W. R. M.; Makimura, Y.; Toghill, K.; Nazar, L. F. *Nat. Mater.* **2007**, *6*, 749.
(16) Marx, N.; , Croguennec, L.; , Carlier, D.; , Suard, E.; , Wattiaux, A.; , F. Le Cras Delmas, C. Submitted to *Dalton Trans.* (Oct. **2009**).
(17) Groat, L. A.; Chakoumakos, B. C.; Brouwer, D. H.; Hoffman, C. M.; Fyfe, C. A.; Morell, H.; Schultz, A. J. *Am. Mineral.* **2003**, *88*, 195.

 Published on Web 01/20/2010

In the frame of this study, a new iron(III) phosphate phase $FePO_4 \cdot H_2O$ was synthesized. Several studies dealing with electrochemical insertion of lithium into hydrated phosphates have been reported so far,[18−24] such as in $FePO_4 \cdot nH_2O$ (with $n = 2$[18,19] and $n = 4$[18]). As especially reported for α-$VOPO_4 \cdot 2H_2O$[24] and $FeVO_4 \cdot nH_2O$,[25] the presence of constitutional and/or surface water in these compounds was shown not to affect their electrochemical performance versus lithium intercalation/deintercalation. Nevertheless, the presence of these water molecules could be a problem regarding the safety. In this paper we will thus report an in-depth chemical and structural characterization of this new iron phosphate-type material, and we will especially focus on the localization of the hydrogen atoms. The first electrochemical tests of lithium batteries using $FePO_4 \cdot H_2O$ as positive electrode material will also be given.

Experimental Section

The $FePO_4 \cdot H_2O$ phase was obtained through a two-step synthesis. The first step consisted of a hydrothermal synthesis of $LiFePO_4(OH)$, this synthesis being described in detail elsewhere.[16] $FePO_4 \cdot H_2O$ (or H_2FeOPO_4) was then obtained from $LiFePO_4(OH)$ (or $HLiFeOPO_4$) through a Li^+/H^+ exchange. A suspension of $LiFePO_4(OH)$ powder was prepared in water and maintained at a moderate temperature (~60 °C), with an excess ($H^+/Li^+ \sim 4$) of nitric acid (65%, J.T. Baker), during 1 week. As expected, the final pH value of the solution was found to be very acidic (pH between 0 and 1). The $FePO_4 \cdot H_2O$ phase thus obtained was pure. Note that the synthesis of this new $FePO_4 \cdot H_2O$ compound can also be done in a methanol or ethanol solution, with the same conditions of reaction (concentration of acid and reaction time). The obtained pale gray-green solid was recovered after filtration and dried at 80 °C overnight. This exchange is, moreover, reversible: a suspension of H_2FeOPO_4 powder in a lithium chloride (LiCl) solution maintained at a moderate temperature (~60 °C) will lead to the formation of $HLiFeOPO_4$ through a H^+/Li^+ exchange. The total deprotonation of the material was tried in order to obtain Li_2FeOPO_4 but without success.

The X-ray diffraction (XRD) pattern was collected at room temperature with a Siemens D5000 powder diffractometer with the Cu Kα radiation in the 2θ range 5−120°, with 2θ step-scan intervals of 0.02° with a constant counting time of 15 s.

Neutron diffraction was performed at the Laue Langevin Institute (ILL) in Grenoble (France) on the high-resolution two-axis powder diffractometer D2B. The diffraction pattern was collected in transmission mode at room temperature with a wavelength of 1.5946(1) Å in the [0−160]° angular range with a 0.05° (2θ) step with an accumulation time of 4 h. The sample was contained in an 8 mm diameter vanadium tube. Due to the geometry of the neutron diffractometer, it was necessary to correct the absorption in order to take into account a decrease of the experimental diffracted intensity compared to the expected one. The calculated absorption correction coefficient (μR factor in the FullProf program) is equal to 0.92 for $FePO_4 \cdot H_2O$. μ is the linear absorption coefficient of the sample and is defined as $\mu = \frac{n}{V}\sum_i n_i\sigma_i$, where n is the number of formula units in the unit cell, V is the cell volume, n_i is the number of a given atom in the formula unit, and σ_i is the sum of coherent and incoherent scattering cross sections for the atom i. R is the radius of the vanadium cylinder. The X-ray and neutron diffraction patterns were analyzed by the Rietveld method as implemented in the FullProf program.[26]

Li, Fe, and P elemental analyses were performed after complete dissolution of the powder into a hydrochloric acid solution, with a Varian 720-ES Optical Emission Spectrometer (ICP-OES). A gas chromatography analysis was also performed with a Thermo Fisher Flash EA1112 CHNS analyzer, in order to quantify the amount of hydrogen in our sample. The water content was determined through a thermogravimetric analysis (TGA), with a TA Instruments Q600 thermogravimetric analyzer.

High Resolution Scanning Electron Microscopy (SEM) analysis of the sample was performed with a Hitachi S-4500 microscope. The powder was metallized by palladium deposition.

Infrared spectroscopy measurements were performed with a FTIR Thermo Optek Nicolet 6700. The spectrometer was equipped with a DTGS detector; a Ge-coated KBr or a solid substrate beamsplitter was used for analyses in the mid-IR or far-IR region respectively. The sampling technique chosen was diffuse reflectance, which allows the study of powder or rough surface. To prevent any distortion of the signal due to its strong dependence on sample particle size, the material to analyze (~1 wt %) was mixed with cesium iodide (CsI) powder that was previously dried at 400 °C overnight and finely ground. CsI was preferred to potassium bromide (KBr) for getting access to middle- and far-infrared (200−4000 cm^{-1}). Finally, reflectance spectra were treated with the Kubelka−Munk law, which converts the reflectance to a signal proportional to the absorption coefficient. Raman scattering measurements were performed with a Horiba Jobin Yvon Labram HR-800 microspectrometer. Spectra were recorded with a 514.5 nm excitation wavelength of an Ar^+ laser, with a power adjusted to 1 mW in order to avoid any degradation of the sample. No specific sample preparation was needed.

For the evaluation of its electrochemical performance in laboratory lithium cells, $FePO_4 \cdot H_2O$ was first ball-milled with a (1:1) mixture of carbon black and graphite (1 g of active material with 210 mg of the carbon mixture during 30 min at 450 rpm), and then PTFE (polytetrafluoroethylene) was added as binder. The final composition of the positive electrode was approximately 80 wt % active material, 17 wt % carbon black/graphite (1:1), and 3 wt % PTFE. The resulting positive electrode was rolled into a thin sheet and cut into 0.64 cm^2 circular disks (containing about 20 mg of active material). Metallic lithium was used as a negative electrode and $LiPF_6$ (1 M) in a mixture of ethylene carbonate (EC), propylene carbonate (PC), and dimethyl carbonate (DMC) in volume proportions 1:1:3 as electrolyte. The batteries were assembled in an argon-filled drybox (H_2O < 3 ppm) and cycled at room temperature in

(18) Masquelier, C.; Reale, P.; Wurm, C.; Morcrette, M.; Dupont, L.; Larcher, D. *J. Electrochem. Soc.* **2002**, *149*(8), A1037.
(19) Zaghib, K.; Julien, C. M. *J. Power Sources* **2005**, *142*, 279.
(20) Song, Y.; Zavalij, P. Y.; Chernova, N. A.; Whittingham, M. S. *Chem. Mater.* **2005**, *17*, 1139.
(21) Dollé, M.; Patoux, S.; Richardson, T. J. *J. Power Sources* **2005**, *144*, 208.
(22) Pralong, V.; Caignaert, V.; Raveau, B. *Solid State Ionics* **2006**, *177*, 2453.
(23) Kishore, M. S.; Pralong, V.; Caignaert, V.; Varadaraju, U. V.; Raveau, B. *J. Power Sources* **2007**, *169*, 355.
(24) Dupré, N.; Gaubicher, J.; Le Mercier, T.; Wallez, G.; Angenault, J.; Quarton, M. *Solid State Ionics* **2001**, *140*, 209.
(25) Poizot, P.; Baudrin, E.; Laruelle, S.; Dupont, L.; Touboul, M.; Tarascon, J. M. *Solid State Ionics* **2000**, *138*, 31.
(26) Rodriguez-Carvajal, J. Laboratoire Léon Brillouin. http://www-llb.cea.fr/fullweb/powder.htm (accessed April 2008).

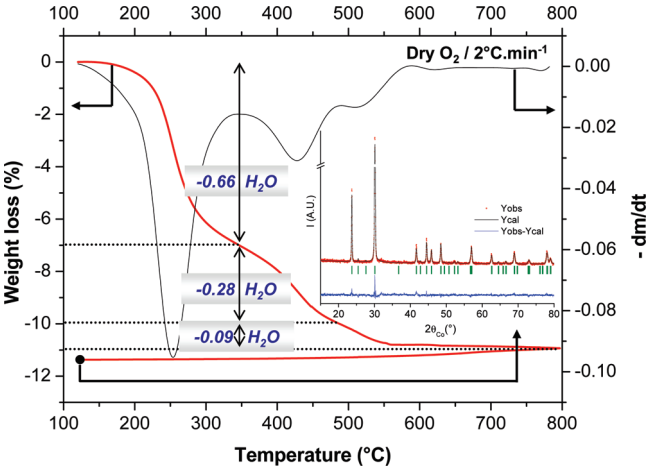

Figure 1. Weight loss curve (and its derivative) observed during the thermogravimetric analysis under dry oxygen of the $FePO_4 \cdot H_2O$ material. The X-ray diffraction pattern recorded for the material recovered after cooling is given in the inset.

galvanostatic mode at a constant C/50 rate (corresponding to a theoretical exchange of one electron per formula during a charge or a discharge in 50 h).

Results and Discussion

Chemical Analysis. In order to confirm the chemical composition of the prepared sample, the Li/P and Fe/P molar ratios were determined using ICP-OES analyses. The latter was found to be 1.03(1), whereas no lithium was detected (concentration below the detection limit), proving that the Li^+/H^+ exchange reaction is complete. The gas chromatography (CHNS) analysis performed revealed the presence of 1.85(5) H per formula unit, which is slightly below the expected content (i.e., 2). With the same idea of confirming the water content in this sample, a TGA analysis was carried out. The material was first heated at 2 °C/min up to 120 °C and maintained at this temperature during 12 h to evaporate the water molecules adsorbed at the surface of the particles. This preliminary weight loss corresponded to 0.54% of the total mass. Then the material was heated at 2 °C/min up to 800 °C. The complete analysis was done under dry oxygen. The weight loss and its derivative are given in Figure 1. $FePO_4 \cdot H_2O$ lost 10.94% of its weight in three steps. Assuming that all the weight loss is associated with structural water, the total loss corresponds to 1.03 H_2O per $FePO_4$. The TGA curve shows clearly the existence of two intermediate hydrated phases of overall formula $FePO_4 \cdot \sim 0.37H_2O$ (obtained at ~350 °C) and $FePO_4 \cdot \sim 0.09H_2O$ (obtained at ~480 °C). These intermediate phases formed at 350 and 480 °C have also been studied; the former was especially fully characterized from a structural and electrochemical point of view: these results will be published elsewhere. The material obtained after complete dehydration of $FePO_4 \cdot H_2O$ (heated up to 800 °C and cooled down to room temperature) was studied by X-ray diffraction. Its pattern is given in the inset in Figure 1 and, as clearly shown by the result of the Rietveld refinement, it corresponds to a quartz α-$FePO_4$ described by the $P3_121$ space group.[27] From all these chemical analyses it appears thus correct to describe the material formed by a Li^+/H^+ exchange from $LiFePO_4$-(OH) as $FePO_4 \cdot H_2O$.

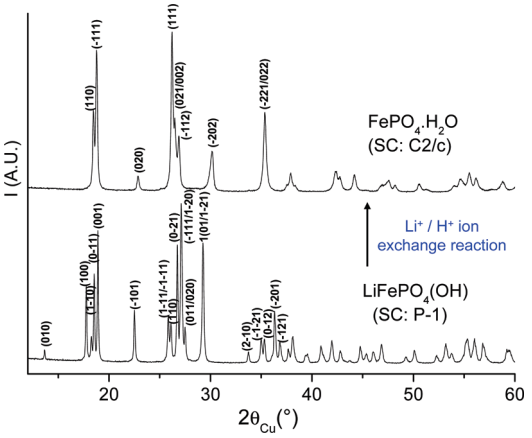

Figure 2. XRD patterns of $LiFePO_4(OH)$ and of the new $FePO_4 \cdot H_2O$ phase.

Table 1. Comparison of the FWHM Values Determined for Three Selected Reflections of the $FePO_4 \cdot H_2O$ XRD Pattern[a]

(*hkl*) indexation	position 2θ (°)	FWHM (°2θ)	*L* (nm)
(110)	18.70	0.19	45
(020)	23.08	0.22	35
(111)	26.41	0.18	50

[a] The coherent domains sizes (L) were roughly estimated using the Scherrer formula.

X-ray Diffraction. The XRD patterns of pure $LiFePO_4$-(OH) and $FePO_4 \cdot H_2O$ phases are compared in Figure 2. The exchange reaction from $LiFePO_4(OH)$ to $FePO_4 \cdot H_2O$ leads to an increase of symmetry from triclinic space group *P*-1 to monoclinic space group *C*2/*c*. The new phase $FePO_4 \cdot H_2O$ could be fully indexed using the *C*2/*c* space group, by analogy with already reported materials $VPO_4 \cdot H_2O$[28] and $MnPO_4 \cdot H_2O$,[29] which are isotypic with our phase. The relatively narrow diffraction peaks suggest that the material is rather well crystallized. The full width at half-maximum (FWHM) of three representative reflections, namely (110), (020), and (111), were determined using a profile fitting software, and the corresponding coherent domains sizes roughly deduced from Scherrer formula[30] are given in Table 1. It suggests that the coherent domain size is rather uniform (around 45 nm) whatever the crystallographic direction. According to the scanning electron micrographs given in Figure 3, the particles have mainly a stick (or platelet) shape and form nonuniform aggregates of about 1−2 μm long and 500 nm thick. On the larger enlargement (perpendicular to the stick) small domains being around 50−100 nm wide appear; they are in the range of the coherent domain size

(27) Long, G. J.; Cheetham, A. K.; Battle, P. D. *Inorg. Chem.* **1983**, *22*, 3012.
(28) Vaughey, J. T.; Harrison, W. T. A.; Jacobson, A. J. *Inorg. Chem.* **1994**, *33*, 2481.
(29) Lightfoot, P.; Cheetham, A. K.; Sleight, A. W. *Inorg. Chem.* **1987**, *26*, 3544.
(30) Scherrer, P. *Göttinger Nachr.* **1918**, *2*, 98.

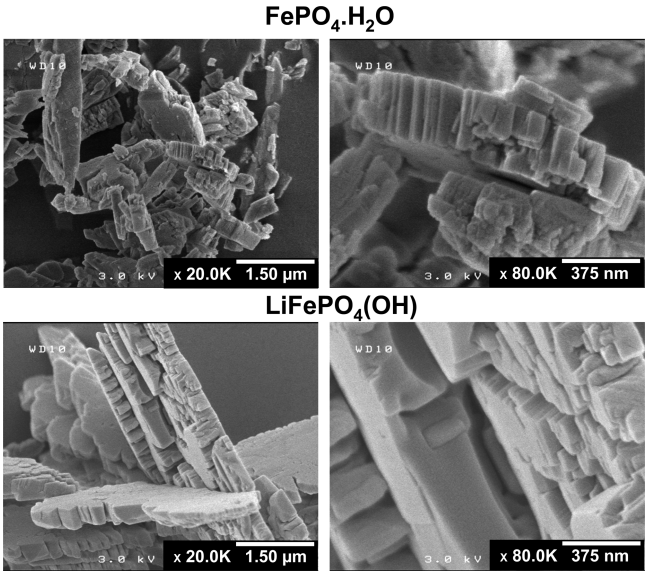

Figure 3. Scanning electron microscopy images of $FePO_4 \cdot H_2O$ in comparison with those of its precursor $LiFePO_4(OH)$.

estimated from a rough analysis of the X-ray diffraction data using the Scherrer formula. Furthermore, the comparison with the SEM micrographs of the precursor $LiFePO_4(OH)$ reveals that the size of the primary particles has been slightly reduced during the exchange reaction in parallel also to a decrease of the coherent domain sizes which was roughly estimated to be around 70 nm for $LiFePO_4(OH)$.[16]

The procedure used to analyze $FePO_4 \cdot H_2O$ powder XRD pattern by the Rietveld method was already described in detail elsewhere.[16] Twenty-nine parameters were refined (on the basis of 292 reflections), considering a polynomial function to model the background and a pseudo-Voigt function to describe the profile. The refinement starting point was the structural model proposed by Vaughey et al. for $VPO_4 \cdot H_2O$[28] (replacing vanadium by iron), i.e. $(Fe)_{4c}\{(P)_{4e}(O(1)_{8f})(O(2)_{8f})\}(O(3))_{4e}$ with the iron atom occupying the special position 4c (1/4, 1/4, 0), the phosphorus atom a 4e (0, y, 1/4) position, two oxygen atoms 8f (x, y, z) positions, and one oxygen atom a 4e (0, y, 1/4) position. Figure 4 gives the result of that refinement: the corresponding agreement factors being R_{wp} = 17.9% and R_{Bragg} = 7.2%. The resulting cell parameters are a = 6.708(2) Å, b = 7.761(2) Å, c = 7.382(2) Å, and β = 115.08(2)° (V = 348.1(2) Å^3).

Neutron Diffraction. In order to localize precisely the H atoms in the $FePO_4 \cdot H_2O$ structure, it was necessary to perform a neutron diffraction study. The main advantage of neutron diffraction is that the scattering factor of H is much greater for neutrons than for X-rays. Moreover, the H atom has a negative coherent scattering length of $-0.3739.10^{-12}$ cm, whereas Fe, P, and O atoms have positives ones, which means that the position of hydrogen will appear with a negative density on Fourier difference maps. In the first step, the refinement of the neutron diffraction pattern by the Rietveld method was carried out by taking into account the structural model $(Fe)_{4c}\{(P)_{4e}(O(1))_{8f}(O(2))_{8f}\}(O(3))_{4e}$ (space group $C2/c$)

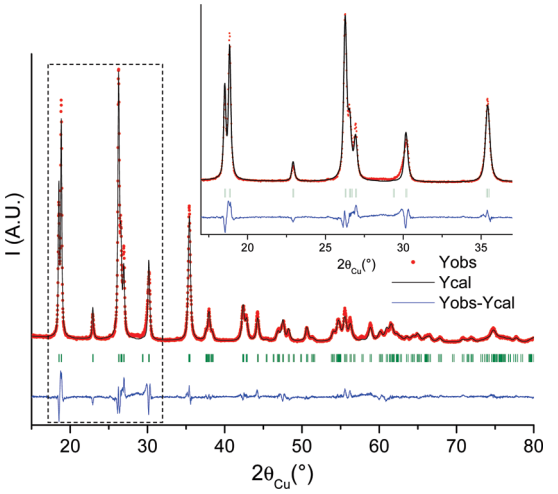

Figure 4. Comparison of the experimental and calculated X-ray diffraction patterns of $FePO_4 \cdot H_2O$. Enlargement of the plot in the range 17−37° (2θ) is given in the inset.

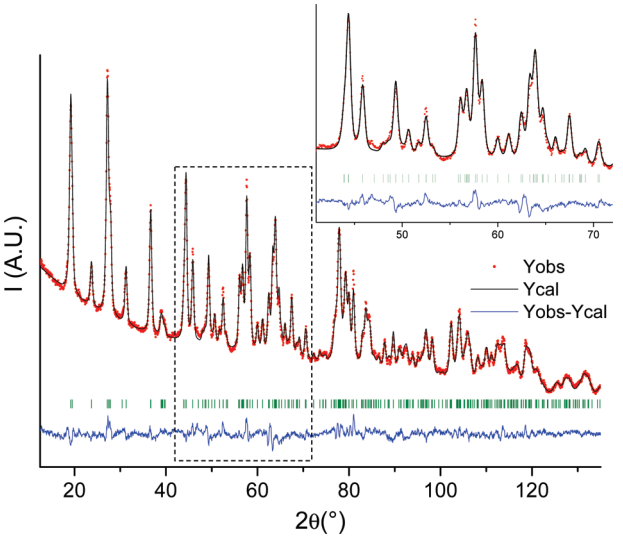

Figure 5. Comparison of the experimental and calculated neutron diffraction patterns. Enlargement of the plot in the range 41−72° (2θ) is given in the inset.

and all structural parameters previously determined from the XRD pattern refinement. As described in detail in ref 16, Fourier difference maps were calculated in order to localize the H atom in the structure. Residual density was found in the 8f position (~0.401, ~0.040, ~0.291). The refined hydrogen position was found to be finally (0.406(4), 0.043(3), 0.295(3)). The result of the neutron diffraction data refinement by the Rietveld method is given in Figure 5. The minimization of the difference (Iobs. − Icalc.) and the quality factors R_{wp} = 9.3% and R_{Bragg} = 4.9% are significantly improved and in fact satisfying. Furthermore, no significant residual nuclear density remained on the Fourier difference map, proving that the structure of $FePO_4 \cdot H_2O$ is solved. The resulting structural parameters are given in Table 2 and the structure representation of $FePO_4 \cdot H_2O$ in Figure 6a. The skeleton of the structure consists of a three-dimensional network, isotypic to that of $LiFePO_4(OH)$ previously

Table 2. Structural and Profile Parameters Obtained by the Rietveld Refinement of the Neutron Diffraction Pattern Recorded for $FePO_4 \cdot H_2O$

space group: $C2/c$

$a = 6.708(2)$ Å

$b = 7.761(2)$ Å $\quad \beta = 115.08(2)°$ $\quad V = 348.1(2)$ Å^3

$c = 7.382(2)$ Å

atom	site	Wyckoff position			occupancy	B_{iso}
Fe	4c	1/4	1/4	0	1	0.9(2)
P	4e	0	0.090(2)	1/4	1	0.7(3)
O(1)	8f	0.205(2)	−0.030(2)	0.348(2)	1	0.9(2)
O(2)	8f	0.035(2)	0.198(1)	0.098(2)	1	1.0(2)
O(3)	4e	0	0.614(2)	1/4	1	1.0(3)
H	8f	0.406(4)	0.043(3)	0.295(3)	1	3.7(4)

Conditions of the Run

wavelength	1.5946(1) Å
temperature	300 K
angular range	$0° \le 2\theta \le 160°$
number of points	3194
zero-shift (2θ)	0.04(2)°
number of fitted parameters	35

Profile Parameters

pseudo-Voigt Function	$\eta = 0.70(6)$
	$U = 0.6(1)$
	V = −0.6(1)
	$W = 0.45(4)$

Conventional Rietveld R-Factors for Points with Bragg Contribution

$R_{wp} = 9.3\%$; $R_{Bragg} = 4.9\%$; Scor = 3.6

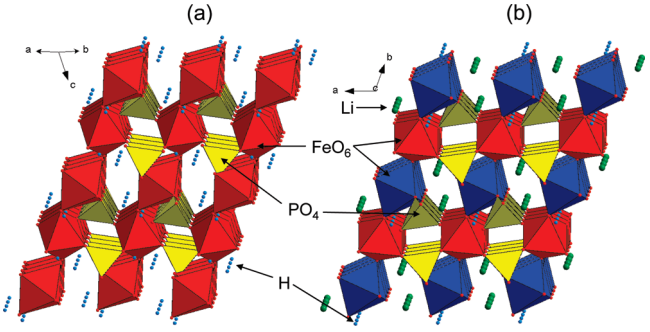

Figure 6. Structures of $FePO_4 \cdot H_2O$ (**a**) and $LiFePO_4(OH)$ (**b**).

described,[16] and given for comparison in Figure 6b. In the $FePO_4 \cdot H_2O$ structure, FeO_6 iron(III) octahedra share corners to form chains running along the [101] direction. These chains are interconnected through PO_4 tetrahedra, such as the resulting framework encloses tunnels running along the [110] and [−110] directions. There is only one type of FeO_6 octahedra, in contrast to $LiFePO_4(OH)$ where two types of FeO_6 octahedra were observed. In the $LiFePO_4(OH)$ structure the chains of FeO_6 octahedra run along the *b* axis and the two tunnels along the *a* and *c* axes. For $FePO_4 \cdot H_2O$, it appears clearly that the two hydrogen atoms are linked to O(3), i.e. to the oxygen bridging two adjacent FeO_6 octahedra. In Table 3, various interatomic distances from both structures are compared. The O−H bond length is equal to 1.00(1) Å and 0.97(1) Å for $FePO_4 \cdot H_2O$ and $LiFePO_4(OH)$, respectively, which is in agreement with literature (0.96 Å for free water) and the H−O(3)−H angle is of 112.6° (104.5° for free water) in $FePO_4 \cdot H_2O$. In $FePO_4 \cdot H_2O$, the phosphorus atom lies within a slightly distorted tetrahedron ($\Delta = 3.8 \times 10^{-4}$) with P−O distances in the range 1.50−1.56 Å, somewhat more distorted than in $LiFePO_4(OH)$ ($\Delta = 4.2 \times 10^{-5}$) with P−O distances in a more narrow range 1.54−1.56 Å. But the main difference between the two structures lies in the FeO_6 octahedra. In $FePO_4 \cdot H_2O$, the iron cations sit within very distorted octahedra ($\Delta = 2.8.10^{-3}$), showing Fe−O distances ranging between 1.91 and 2.17 Å, and especially elongated along the FeO_6 chains. These FeO_6 octahedra are much more distorted than those observed in $LiFePO_4(OH)$ (Δ Fe(1)$O_6 = 1.7 \cdot 10^{-5}$ with Fe−O distances in the range 2.00−2.02 Å and Δ Fe(2)$O_6 = 2.7 \cdot 10^{-4}$ with Fe−O distances between 1.96 and 2.03 Å). There are two main reasons why there is a difference in the structures distortion. First, the presence of two H atoms linked to the bridging oxygen atom O(3) in $FePO_4 \cdot H_2O$, instead of only one in $LiFePO_4(OH)$, forming a "H_2O-like isolated molecule", considerably weakens the Fe−O(3) bond (along the FeO_6 chain), thus leading to a strong elongation of this bond. Second, the overall lattice, made of corner sharing polyhedra, can easily be distorted to facilitate the hydrogen bond formation. Thus, as shown in Figure 7, in $FePO_4 \cdot H_2O$ the hydrogen atom is very close to the O(1) oxygen atom, leading to the formation of a hydrogen bond, that must be quite intense as a result of the short H···O distance (1.65 Å). Whereas in $LiFePO_4(OH)$ the formed hydrogen bonds are slightly weaker in good agreement with less distorted polyhedra, since the distance to the second nearest oxygen is longer (~1.86 Å), and also less numerous, since half of the hydrogen atoms are replaced by lithium ones (in comparison to $FePO_4 \cdot H_2O$). One has also to consider that the larger size of the Li^+ ions (the

Table 3. Interatomic Distances in $FePO_4 \cdot H_2O$ and $LiFePO_4(OH)$[a]

	$FePO_4 \cdot H_2O$		$LiFePO_4(OH)$	
FeO_6	Fe−O(2) (×2)	1.91(2) Å	Fe1−O(2) (×2)	2.00(2) Å
	−O(1) (×2)	2.00(2) Å	−O(4) (×2)	2.01(2) Å
	−O(3) (×2)	2.17(2) Å	−O(3) (×2)	2.02(2) Å
	Average (⟨*d*⟩)	2.03 Å	***Average*** (⟨*d*⟩)	2.01 Å
	Distorsion (Δ)	2.8×10^{-3}	***Distorsion*** (Δ)	1.7×10^{-5}
			Fe2−O(2) (×2)	1.96(2) Å
			−O(4) (×2)	2.03(2) Å
			−O(3) (×2)	2.03(2) Å
			Average (⟨*d*⟩)	2.01 Å
			Distorsion (Δ)	2.7×10^{-4}
PO_4	P−O(2) (×2)	1.50(2) Å	P−O(5)	1.54(2) Å
	−O(1) (×2)	1.56(2) Å	−O(4)	1.54(2) Å
	Average (⟨*d*⟩)	1.53 Å	−O(2)	1.56(2) Å
	Distorsion (Δ)	3.8×10^{-4}	−O(1)	1.56(2) Å
			Average (⟨*d*⟩)	1.55 Å
			Distorsion (Δ)	4.2×10^{-5}
OH	O(3)−H	1.00(1) Å	O(3)−H	0.97(1) Å
2nd nearest O	O(3)−H···O(1)	1.65(2) Å	O(3)−H···O(1)	1.86(2) Å
HH	H−H (same O(3))	1.66(2) Å	H−H (tunnel)	2.65(2) Å
	H−H (tunnel)	2.82(2) Å		
Li environment (LiO_5)			Li−O(3)	1.94(2) Å
			−O(1)	2.03(2) Å
			−O(2)	2.05(2) Å
			−O(5)	2.16(2) Å
			−O(1)'	2.22(2) Å
			Average(⟨*d*⟩)	2.08 Å
			Distortion (Δ)	2.3×10^{-3}

[a] Distortion calculated with the formula $\Delta = \frac{1}{N}\sum_{i=1}^{N}\left(\frac{d_i - \langle d\rangle}{\langle d\rangle}\right)^2$, where d_i is the length of the bond i, $\langle d\rangle$ is the average bond length, and N is the number of bonds.

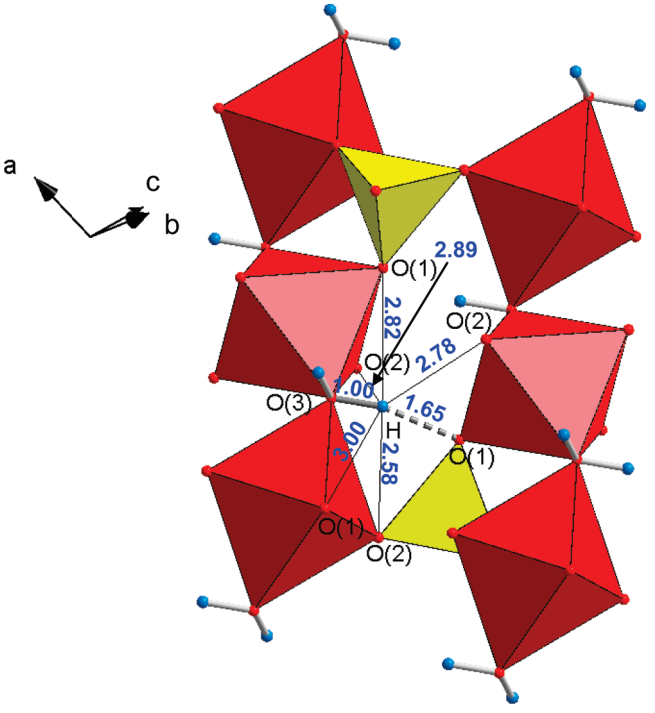

Figure 7. Environment of the H atom in $FePO_4 \cdot H_2O$, the H−O distances being smaller than 3.0 Å are given.

Li−O bond length is close to 2 Å) prevents from a large cooperative framework distortion.

IR-Raman. Infrared spectroscopy and Raman scattering studies were performed on both $FePO_4 \cdot H_2O$ and $LiFePO_4(OH)$ in order especially to get additional information on their local structures. At the Brillouin zone center, the decomposition of optical normal vibrations by irreducible representations of the factor group C_{2h} for $FePO_4 \cdot H_2O$ and C_i for $LiFePO_4(OH)$ are given in Table 4. Theoretically, 27 IR-active modes and 24 Raman-active modes are expected for both materials.

Table 4. Results of the Factor Group Analysis for $FePO_4 \cdot H_2O$ and $LiFePO_4(OH)$[a]

$FePO_4 \cdot H_2O$, factor group C_{2h}	$LiFePO_4(OH)$, factor group C_i
$\Gamma_{opt} = 11A_g + 13B_g + 13A_u + 14B_u$	$\Gamma_{opt} = 24A_g + 27A_u$

[a] ≪ gerade ≫ and ≪ ungerade ≫ species are respectively Raman-active and infrared-active modes.

The spectra were recorded in the range 200−4000 cm^{-1}, those corresponding to diffuse reflectance infrared spectroscopy are given in Figure 8a and those for Raman scattering in Figure 8b. Spectral assignments for some of the phosphates ($LiFePO_4$, $FePO_4$ heterosite) vibrations have already been reported.[31−35] The observed bands can be divided into different domains: the region above 2300 cm^{-1} is assigned to the OH stretching bands; the domain from 900 to 1200 cm^{-1} is attributed to the PO_4 stretching bands; the band around 800 cm^{-1} remains up to now not

(31) Paques-Ledent, M. T.; Tarte, P. *Spectrochim. Acta, Part A* **1974**, *30*, 673.
(32) Burba, C. M.; Frech, R. *J. Electrochem. Soc.* **2004**, *151*(7), A1032.
(33) Burba, C. M.; Frech, R. *Spectrochim. Acta, Part A* **2006**, *65*, 44.
(34) Ait Salah, A.; Jozwiak, P.; Zaghib, K.; Garbarczyk, J.; Gendron, F.; Mauger, A.; Julien, C. M. *Spectrochim. Acta, Part A* **2006**, *65*, 1007.
(35) Maccario, M.; Croguennec, L.; Desbat, B.; Couzi, M.; Le Cras, F.; Servant, L. *J. Electrochem. Soc.* **2008**, *155*(12), A879.

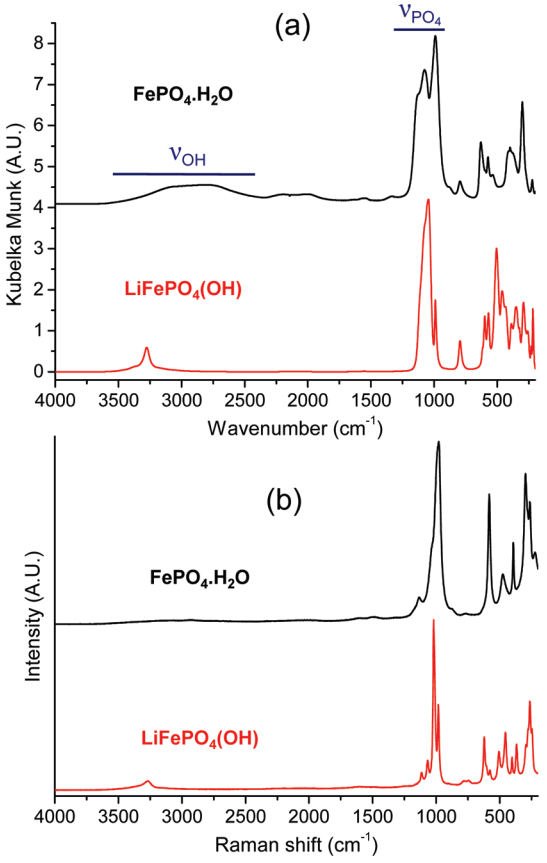

Figure 8. Comparison of the infrared (**a**) and Raman (**b**) spectra for $FePO_4 \cdot H_2O$ and $LiFePO_4(OH)$.

clearly explained, but could be attributed to the Fe−O stretching bands in case of a Fe−O−H sequence; then the region from 350 to 600 cm^{-1} is assigned together to the PO_4 bending bands and to the vibrations of Fe−O and Li−O units; and finally the domain below 350 cm^{-1} is assigned to the lattice vibrations. Concerning the last two domains, a more accurate attribution would be tricky; therefore, they will not be discussed here.

In order to facilitate the analysis of the spectra dominated by the PO_4 stretching bands in the region from 900 to 1200 cm^{-1}, a factor group analysis was performed for these modes, correlating the point group of the free PO_4 ion with the phosphate site and factor groups for both $FePO_4 \cdot H_2O$ and $LiFePO_4(OH)$. This scheme is given in Table 5. The symmetric stretching mode (ν_1) of the "free" PO_4 ion generates a band in IR and Raman spectra, and the antisymmetric stretching mode (ν_3) splits into three components. The spectra in the range of this $\Delta\nu_3$ splitting ($\Delta\nu_3$ being the difference in frequencies between the highest and lowest ν_3 bands) were fitted using pseudo-Voigt bands (see also Figure SI as Supporting Information); the positions and assignments of the calculated bands are gathered in Table 5. It appears clearly that the $\Delta\nu_3$ splitting is larger in $FePO_4 \cdot H_2O$ ($\Delta\nu_3$ = 103 and 130 cm^{-1}, respectively, for IR and Raman spectroscopy) than in $LiFePO_4(OH)$ ($\Delta\nu_3$ = 69 and 96 cm^{-1}, respectively, for IR and Raman spectroscopy). As reported in Table 3, the PO_4 tetrahedra are about 10 times more distorted in $FePO_4 \cdot H_2O$ than in $LiFePO_4(OH)$. Furthermore, as previously mentioned, the FeO_6 octahedra are also much more distorted in $FePO_4 \cdot H_2O$ in comparison to $LiFePO_4(OH)$, influencing the PO_4 tetrahedra distortion. The splitting of the PO_4^{3-} internal modes (in the $A^{I}B^{II}X^{V}O_4$ materials) is mainly related to "an unequal distribution of the bonding forces within the tetrahedral group" [31]; we linked it to the distortion of the PO_4 tetrahedra.

As already discussed before, the distances between the H atoms and the second nearest oxygen are rather short (<2 Å) in both materials, thus allowing the presence of hydrogen bonds having a strong influence on the FeO_6 octahedra and PO_4 tetrahedra distortion, especially in $FePO_4 \cdot H_2O$. The observation of the OH stretching bands domain reveals that the narrow bands observed around 3300 cm^{-1} for $LiFePO_4$-(OH) in both infrared and Raman scattering spectra are typical of hydroxyl groups influenced by their environments (when the OH group is isolated the band appears at a higher wavenumber *i.e.* between 3500 and 3700 cm^{-1} [36]); however, the narrow profile of the band indicates that the hydrogen bonds are quite weak in this material. On the contrary, the large band from 2300 to 3500 cm^{-1} observed for $FePO_4 \cdot H_2O$ in infrared spectroscopy, combined to extremely weak signals at high frequencies in Raman scattering is consistent with OH_2 groups in this material. The large profile of the band indicates in this case the presence of hydrogen bonds. These observations were confirmed by ATR (Attenuated Total Reflectance) measurements, for which the material is analyzed without sample preparation, proving thus that the observations made above 2300 cm^{-1} cannot be attributed to hydrated CsI powder but to the samples studied.

Electrochemical Tests in Li Batteries. $FePO_4 \cdot H_2O$ was tested as positive electrodes in laboratory Swagelock-type lithium batteries. The stability of the material in the presence of the electrolyte was checked: after 2 weeks the X-ray diffraction pattern remained unchanged; the reversible H^+/Li^+ ion exchange does not occur at room temperature. Figure 9 gives the changes in voltage versus the Li content in $FePO_4 \cdot H_2O$ and the capacity during the first galvanostatic charge/discharge cycles performed between 2 and 4.5 V (vs Li^+/Li) at a C/50 rate. The average potential is ~2.8 V vs Li^+/Li (lower than the potential of the Fe^{3+}/Fe^{2+} redox couple in olivine $LiFePO_4$, i.e. 3.45 V vs Li^+/Li) with a capacity of 125 mAh·g^{-1} for the first discharge that stabilizes at 105 mAh·g^{-1} for the next cycles but in nonoptimized conditions from the point of view of the electrodes and lithium cells. In comparison, as reported by some of us in ref 16 the Li//$LiFePO_4$(OH) cell shows a capacity of 105 mAh·g^{-1} for the first discharge, decreasing to 90 mAh·g^{-1} for the next cycles with an average potential around 2.4 V vs Li^+/Li. The polarization is high (~500 mV) for $FePO_4 \cdot H_2O$ and larger than for $LiFePO_4(OH)$ (~200−300 mV). The change in potential versus the lithium content is more or less continuous. Nevertheless, the derivative of the first charge/discharge cycle is given in the inset in order to get a deeper

(36) Nakamoto, K. Infrared and Raman Spectra of Inorganic and Coordination Compounds, Part A: Theory and Applications in Inorganic Chemistry, Wiley-Interscience, John Wiley & Sons, Inc.: 1997; p 161.

Table 5. Correlation Scheme for the Stretching Modes of PO_4^{3-} Units and Observed Infrared and Raman Bands Assigned to These Modes for Both $FePO_4 \cdot H_2O$ and $LiFePO_4(OH)$

free PO_4			$FePO_4 \cdot H_2O$			$LiFePO_4(OH)$			
stretching modes	point group T_d	site group C_2	factor group C_{2h}	assignment	wavenumber (cm^{-1})	site group C_1	factor group C_i	assignment	wavenumber (cm^{-1})
symmetric mode (ν_1)	A_1	A	$A_g + A_u$	$A_{g\text{-}\nu1}$ $A_{u\text{-}\nu1}$	980 988	A	$A_g + A_u$	$A_{g\text{-}\nu1}$ $A_{u\text{-}\nu1}$	983 989
antisymmetric mode (ν_3)	F_2	A + 2B	$A_g + A_u + 2B_g + 2B_u$	$A_{g-\nu3}$ $2B_{g-\nu3}$	1004 1041 1134 ($\Delta\nu_3 = 130$)	3A	$3A_g + 3A_u$	$A_{g\text{-}\nu3}$	1018 1067 1114 ($\Delta\nu_3 = 96$)
				$A_{u-\nu3}$ $2B_{u-\nu3}$	1032 1077 1135 ($\Delta\nu_3 = 103$)			$A_{u\text{-}\nu3}$	1042 1077 1111 ($\Delta\nu_3 = 69$)

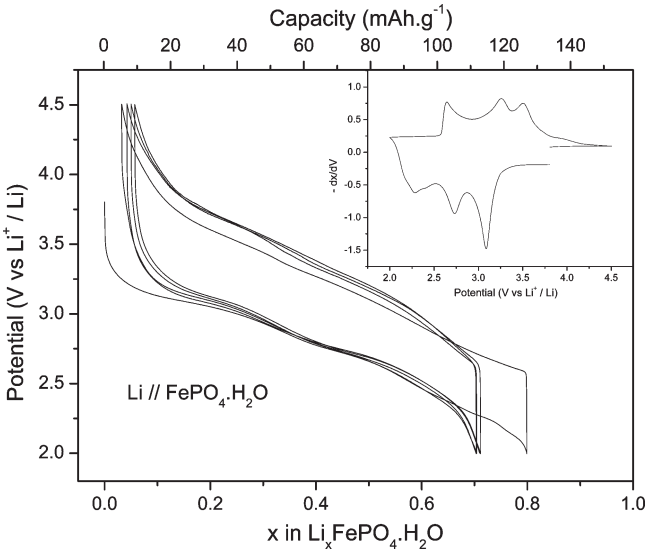

Figure 9. The first electrochemical cycles observed for a Li//$FePO_4 \cdot H_2O$ cell, cycled between 2.0 and 4.5 V (vs Li^+/Li) at a C/50 rate. The derivative of the first discharge/charge cycle is given in the inset.

insight in the possible transitions occurring upon cycling: during the first discharge of the cell, three transitions are observed around 3.09, 2.73, and 2.28 V (vs Li^+/Li). These transitions seem to be reversible since three transitions are also observed during the first charge of the cell around 2.64, 3.26, and 3.51 V (vs Li^+/Li). Furthermore, because of the broad shape of the derivative peaks, we can assume that these transitions are of second order. Note that the electrochemical lithium intercalation mechanism in $FePO_4 \cdot H_2O$ is really different from that in $LiFePO_4(OH)$; the first one seems to occur through a solid solution reaction, whereas the second one occurs through a first order phase transition suggesting an irreversible structural modification during the first discharge. These mechanisms are currently under study, for instance through combined X-ray diffraction and electrochemical experiments.

Conclusions

The synthesis of a new hydrated form of $FePO_4 \cdot nH_2O$ with $n = 1$ was reported here, and it was obtained through a Li^+/H^+ exchange in $LiFePO_4(OH)$. Its structure was shown to be very similar to that of $LiFePO_4(OH)$, but with differences in the distortion of the chains and of the polyhedra, those being responsible for a change in symmetry from a triclinic (P-1) to a monoclinic ($C2/c$) space group. The hydrogen atoms were precisely located in the $FePO_4 \cdot H_2O$ structure; they were shown to be bound to the oxygen atoms bridging two adjacent FeO_6 octahedra in the chains (leading to the formation of a "H_2O-like molecule" that leads to a significant distortion of the FeO_6 octahedra) and to formation of a strong hydrogen bond with an oxygen from an adjacent chain, that hydrogen bond being stronger than that observed in $LiFePO_4(OH)$. Despite rather similar structures, these significant differences, revealed through an in depth characterization done using diffraction and vibrational spectroscopy, are probably responsible for the different electrochemical behavior observed for $FePO_4 \cdot H_2O$ and its precursor $LiFePO_4(OH)$.

Acknowledgment. The authors would like to thank CEA, ADEME, and the Région Aquitaine for their financial support, ILL for the neutron diffraction experiment, Emmanuelle Suard (ILL-Grenoble) for her technical assistance during the neutron diffraction experiments, Michel Couzi (ISM) for the IR-Raman fruitful discussions, and Benoit Armand, Philippe Dagault, Cathy Denage, and Jérémy Humez (ICMCB-CNRS) for their technical assistance.

Supporting Information Available: Fitting results, using a pseudo-Voigt function, of the infrared and Raman spectra for $FePO_4 \cdot H_2O$ and $LiFePO_4(OH)$ in the PO_4^{3-} stretching region. This material is available free of charge via the Internet at http://pubs.acs.org.